

Master Thesis

Resonant Raman spectra of LaAlSi using
linearly and circularly polarized light
(直線および円偏光を用いたLaAlSiの共鳴ラマン
スペクトル)

Wang Tong

Department of Physics, Graduate School of Science
Tohoku University

July 2020

Acknowledgments

In this opportunity, I would like to express my appreciate to everyone who supported me to finish my master course and thesis. Firstly, I would like to say thanks to Prof. R. Saito, my supervisor. In these past two years, Saito-sensei helped me to go to my new research field Raman spectra. He also taught me the correct attitude on doing research. Meanwhile, I would like to appreciate our assistant professor Nguyen T. Hung. Nguyen-san taught me a lot both on research and life, and also shared new advanced topics with me, which made me have a comprehensive view in the science world. And also Pang-san and Tian-san, who are Chinese students and came to Japan at the same time with me, they shared a lot of information with me which helped me have an easier life. Shoufie-san, Pratama-san and Wang Sake-san always give me a lot of good suggestions to my research on the group seminar.

Finally, I also appreciate Tohoku University and MEXT scholarship that support my study in Japan. I appreciate GP-MS program who gave me a chance to communicate with excellent researchers in different fields and also will support my doctor course.

Contents

Acknowledgments	iii
Contents	v
1 Introduction	1
1.1 Purpose of the study	1
1.2 Organization of the Thesis	2
1.3 Background	2
1.3.1 Raman spectra	3
1.3.2 Linearly polarized light Raman spectra	4
1.3.3 Circular polarized light Raman spectra	8
1.3.4 Conservation law	11
1.3.5 Weyl semimetal	12
1.3.6 Experimental Results of resonant Raman spectra for LaAlSi	14
2 Methods of calculating resonant Raman intensity	17
2.1 Raman intensity	17
2.2 Electron-photon interaction by DFT	18
2.3 Electron-phonon interaction by DFT	19
2.4 Raman tensor	20
3 Resonant Raman spectra of LaAlSi	23
3.1 Electronic properties of LaAlSi	23
3.2 Polarized Raman spectra	25
3.3 Phonon frequency shift	28

3.3.1	Kohn anomaly effect	28
3.3.2	Breit-Wigner-Fano effect	30
3.4	Circularly polarized Raman spectra	31
4	Conclusions	33
A	Input files for electron-photon and electron-phonon interaction matrix element	35
A.0.1	Input files based on Quantum espresso	36
	Bibliography	49

Chapter 1

Introduction

1.1 Purpose of the study

Raman spectra is a useful technique to characterize the lattice structure, electronic properties and phonon properties [1, 2, 3, 4]. In this thesis, we would like to study electron-photon and electron-phonon interactions of the Weyl semimetal(WSM) material LaAlSi with using linearly and circularly polarized light. The WSM is one kind of emerging materials with the Weyl nodes and the Fermi arcs[5, 6, 7], which attracted lots of interests in recent years. In our research, we investigated the Raman spectra of the WSM which is used to study the symmetry of phonon modes for the WSM. In order to get the Raman Intensity, density functional theory (DFT)[8, 9], which is used to calculating the ground states of electrons and get the wave functions, is the basis for solving the electron-photon and electron-phonon interactions numerically. The purpose of present thesis is to explain the phonon symmetry properties of the WSM by using the first-order resonant Raman spectra.

The material LaAlSi/LaAlGe [10, 11, 12] belongs to the WSM which received a lot of interests in recent years. In this thesis, we will investigate the resonant Raman spectra of LaAlSi combined theoretical analysis with experimental results. Firstly, the laser energy dependence is explored by the polarized Raman spectra. In the experimental results, phonon frequency showed some irregular phenomenons in the Raman process. We will explain the possible reason of frequency shift in addition to the basic angle-dependent Raman spectra. Furthermore, circularly polarized light was used as

the light source of resonant Raman spectra. Tatsumi pointed out that the conservation law of angular momentum existing in the resonant Raman process with circular polarized light[13]. He predicted the possible materials which have helicity changing behavior theoretically. However, there is still no experimental people worked on circularly polarized Raman spectra for the four-fold symmetry and two-fold symmetry materials. In this thesis, we will verify this theory by using the circularly polarized Raman spectra for four-fold material LaAlSi, numerically.

1.2 Organization of the Thesis

This master thesis is organized as follows: there are four chapters. In Chapter 1, we give the the purpose of this thesis, and show backgrounds which consist of Raman process, conservation law, Weyl semimetal and the experimental results of resonant Raman spectra for LaAlSi (S. Huang's group). In Chapter 2, we will present the method of calculation. Meanwhile, introduce the open source software and our home-made program. In Chapter 3, we discuss the polarized Raman spectra of LaAlSi by using five laser energies. Meanwhile, we explain the circularly polarized Raman spectra of LaAlSi and corresponding phonon modes behavior. In Chapter 4, we show conclusions about this thesis.

1.3 Background

When light is scattered by materials, the Raman and Rayleigh scattering both occur. The Rayleigh scattering is an elastic scattering of light which occurs with a relatively higher probability; On the other hand, the Raman scattering is an inelastic scattering.[14] There are two types of Raman scattering: the Stokes and anti-Stokes Raman scattering [15, 16]. If the energy of the scattered light is smaller(larger) than that of the incident light, the scattering is called the Stokes(anti-Stokes) Raman scattering. In this thesis, we discuss only on the Stokes Raman scattering.

In this section, we will explain the Raman process, linearly [17, 18] and circularly polarized light Raman spectra [19, 20], and introduce Weyl semimetal LaAlSi. Meanwhile, explain the experimental results of the Raman spectra for LaAlSi. The

derivation of equations for the Raman intensity which is shown in this chapter will be explained in Chapter 2.

1.3.1 Raman spectra

The schematic diagram of the Raman scattering is shown in Fig.1.1. The initial state is i state. When the incident light is coming, an electron is excited from the i state of valence band to the intermediate state (m) of conduction band by electron-photon interaction. This is the absorption process. If the energy of incident light is identical to energy difference of i state and m state, we called this resonance Raman scattering. Then this photon excited electron is scattered to intermediate state (m') and a phonon is emitted by the electron-phonon interaction. Next step is that the electron recombines with a hole by emitting a photon. The energy difference between the incident light and scattered light is the energy of the emitted phonon.

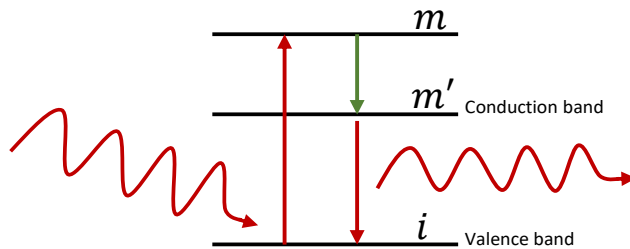


Figure 1.1 The schematic diagram of Raman scattering process, which includes two electron-photon and one electron-phonon interactions. The red lines are the electron-photon interactions, the green line is the electron-phonon interaction.

In this thesis, we mainly focus on the first-order Raman spectra. In this case, the momentum of the emitted phonon is almost zero, and the electrons have no momentum changing in the Raman process. This means that we will only consider the candidate of phonons at the Γ point in the Brillouin zone.

In next section, we will introduce the linearly and circularly polarized Raman spectra. Meanwhile, explain how the polarized light interacts with matter in the Raman spectra combined both group theory analysis and experimental results[21, 22].

1.3.2 Linearly polarized light Raman spectra

When the linearly polarized light is used as the light source, the schematic diagram of the Raman spectra is shown in Fig. 1.2. In this process, the direction of propagation for incident and scattered light are k_i and k_s respectively, which are perpendicular to the xy plane. The polarized vector P_i and P_s are both in the xy plane. Here, θ and φ are polarized angles of incident and scattered light.

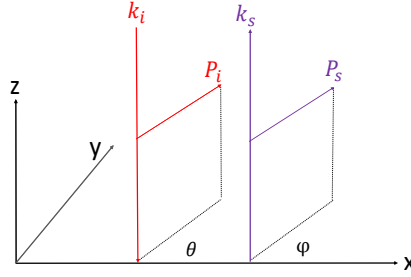


Figure 1.2 Schematic diagram of Raman spectra by using a linearly polarized light. k_i and k_s are the direction of propagation for incident and scattered light. P_i and P_s are polarized vectors. θ and φ are polarized angles.

The polarized vectors of incident and scattered light are defined by:

$$P_i = \begin{pmatrix} \cos \theta \\ \sin \theta \\ 0 \end{pmatrix}, \quad (1.1)$$

$$P_s = \begin{pmatrix} \cos \varphi \\ \sin \varphi \\ 0 \end{pmatrix}, \quad (1.2)$$

Then, we will discuss the resonant Raman spectra in parallel ($Z(X\bar{X})\bar{Z}$) and perpendicular configuration ($Z(X\bar{Y})\bar{Z}$) combined with group theory analysis.

In order to analyze the Raman spectra simply, the analysis expression of Raman intensity is needed, which is written by:

$$I = |P_s^* \cdot R \cdot P_i|^2 \quad (1.3)$$

where R and P_i (P_s) are the Raman tensor and the polarized vectors of incident (scattered) light.

The Raman tensor in Eq.1.3 is given by the character table of the point group [23]. For MoS₂, the Raman tensor of the Raman active modes (E_{2g}^1 and A_{1g}) are denoted by $R(E_{2g}^1(xy), E_{2g}^1(x^2 - y^2))$ and $R(A_{1g}(x^2 + y^2, z^2))$, respectively. And they are given by:

$$R(E_{2g}^1(xy), E_{2g}^1(x^2 - y^2)) = \begin{pmatrix} 0 & d' & 0 \\ d' & 0 & 0 \\ 0 & 0 & 0 \end{pmatrix}, \begin{pmatrix} d & 0 & 0 \\ 0 & -d & 0 \\ 0 & 0 & 0 \end{pmatrix}. \quad (1.4)$$

$$R(A_{1g}(x^2 + y^2, z^2)) = \begin{pmatrix} a & 0 & 0 \\ 0 & a & 0 \\ 0 & 0 & b \end{pmatrix}. \quad (1.5)$$

For the parallel geometry, the polarizd angles of incident light equal to the polarizd angles of scattered light($\theta = \varphi$), then the P_i and P_s are written as:

$$P_i = P_s = \begin{pmatrix} \cos \theta \\ \sin \theta \\ 0 \end{pmatrix} \quad (1.6)$$

By putting the Eq.(1.4), (1.5) and (1.6) into Eq.(1.3), the Raman intensity for the E_{2g}^1 and A_{1g} mode are given by

$$I(E_{2g}^1(xy)) = \left| \begin{pmatrix} \cos \theta & \sin \theta & 0 \end{pmatrix} \begin{pmatrix} 0 & d' & 0 \\ d' & 0 & 0 \\ 0 & 0 & 0 \end{pmatrix} \begin{pmatrix} \cos \theta \\ \sin \theta \\ 0 \end{pmatrix} \right|^2 \\ = |d' \sin 2\theta|^2 \quad (1.7)$$

$$I(E_{2g}^1(x^2 - y^2)) = \left| \begin{pmatrix} \cos \theta & \sin \theta & 0 \end{pmatrix} \begin{pmatrix} d & 0 & 0 \\ 0 & -d & 0 \\ 0 & 0 & 0 \end{pmatrix} \begin{pmatrix} \cos \theta \\ \sin \theta \\ 0 \end{pmatrix} \right|^2 \\ = |d \cos 2\theta|^2 \quad (1.8)$$

$$\begin{aligned}
I(A_{1g}(x^2 + y^2, z^2)) &= \left| \begin{pmatrix} \cos \theta & \sin \theta & 0 \end{pmatrix} \begin{pmatrix} a & 0 & 0 \\ 0 & a & 0 \\ 0 & 0 & b \end{pmatrix} \begin{pmatrix} \cos \theta \\ \sin \theta \\ 0 \end{pmatrix} \right|^2 \\
&= |a|^2
\end{aligned} \tag{1.9}$$

By analyzing the Raman intensity, E_{2g}^1 mode shows four-fold symmetry with considering the intensity which are proportional to $|\sin 2\theta|^2$ and $|\cos 2\theta|^2$. For the A_{1g} mode, the intensity is a constant a^2 , which is an invariant as a function of polarized angle. As shown in Fig.(1.3), $E_{2g}^1(xy)$ mode has the maxma intensity at 45 and 135 degree, and the major peak of $E_{2g}^1(x^2 - y^2)$ appears at 0 and 90 degree. The $A_{1g}(x^2 + y^2, z^2)$ mode is circle plot. We conclude the E_{2g}^1 is four-fold symmetry and the A_{1g} mode has a circle plot.

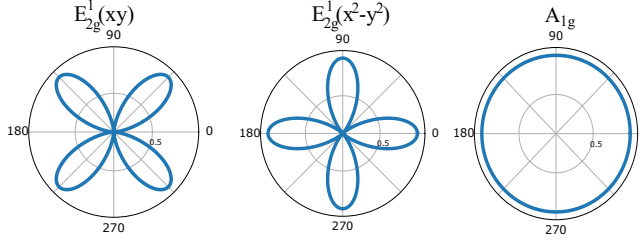


Figure 1.3 Polar plot of the E_{2g}^1 and A_{1g} mode under parallel configuration. In this plot, we assume $d' = d = a = 1$.

In the previously section, we discussed the parallel configuration of the incident and scattered light. For the crossing configuration, which means the polarized vectors of incident light and scattered light are perpendicular to each other, the angle $\varphi = \theta + \frac{\pi}{2}$. In this case, the polarized vectors are given by:

$$P_i = \begin{pmatrix} \cos \theta \\ \sin \theta \\ 0 \end{pmatrix} \tag{1.10}$$

$$P_s = \begin{pmatrix} \cos(\theta + \frac{\pi}{2}) \\ \sin(\theta + \frac{\pi}{2}) \\ 0 \end{pmatrix} = \begin{pmatrix} -\sin \theta \\ \cos \theta \\ 0 \end{pmatrix} \quad (1.11)$$

Combined with Eq.(1.3), the intensity of the E_{2g}^1 and A_{1g} mode are ($|d' \cos 2\theta|^2$, $|-d \sin 2\theta|^2$) and 0, respectively. The intensity of the A_{1g} mode becomes zero in the crossing configuration. By changing the configuration of the Raman process, the A_{1g} mode can be distinguished.

By analyzing the configuration of incident and scattered light, we explained of phonon symmetry for the E_{2g}^1 and A_{1g} mode of MoS_2 . However, in the experiment, the resonant Raman spectras show laser energy and layer dependence, which can not be explained by group theory analysis.

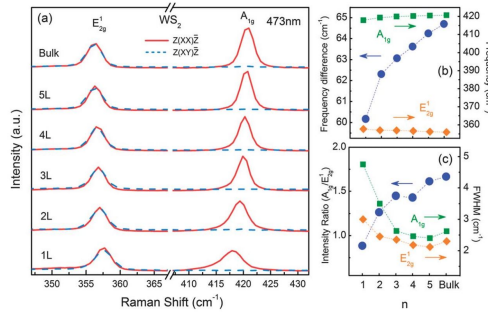


Figure 1.4 (a) Raman spectra of 1-5L and bulk WS_2 flakes in parallel ($Z(XX)\bar{Z}$) and cross ($Z(XY)\bar{Z}$) configuration. (b) Position of the E_{2g}^1 and A_{1g} mode as a function of number of layers. (c) Intensity ratio of the E_{2g}^1 and A_{1g} mode as a function of the number of layers.

[24]

In Fig. 1.4, we show the experimental resonant Raman spectra of WS_2 by using the parallel and cross configurations[24]. The Raman tensors of the E_{2g}^1 and A_{1g} mode have the same form with MoS_2 . For the E_{2g}^1 mode, the peak is both allowed in parallel and cross configuration. And for the A_{1g} mode, it is only allowed with parallel configuration. Thus, the A_{1g} mode can be identified by changing configuration. Furthermore, in Fig. 1.4(b), the frequency of the A_{1g} mode is modified by changing the layer of materials. Meanwhile, the intensity ratio of the E_{2g}^1 and A_{1g} mode become a function of the layer in Fig. 1.4(c).

By analyzing the Raman tensor which derived from group theory, the basic symmetry of phonon modes is revealed. However, the resonant Raman spectra is more complicated that related to the laser energy, the thickness and other parameters. In this case, how to use quantum theory to calculate the Raman tensor becomes an important topic.

1.3.3 Circular polarized light Raman spectra

Compared with linearly polarized light, the circularly polarized light [25] leads to unusual behaviors for phonon modes in Raman process. In this section, we will introduce the circularly polarized Raman spectra and explain how it works in the Raman spectra. Meanwhile, the conservation law of helicity Raman spectra will be introduced.

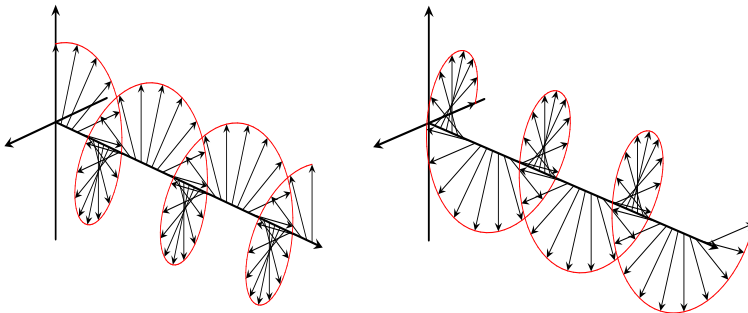


Figure 1.5 The left (right) figure is left (right) -handed circularly polarized light.

Circular polarized light, which has a spin angular momentum $\pm\hbar$, plays an important role in the Raman spectra. In Fig.1.5, we show both left- and right- handed polarized light. The polarization vectors of left/right-handed polarized light are given by:

$$\sigma_{+} = \begin{pmatrix} 1 \\ i \\ 0 \end{pmatrix}. \quad (1.12)$$

$$\sigma_- = \begin{pmatrix} 1 \\ -i \\ 0 \end{pmatrix}. \quad (1.13)$$

With the circularly polarized vectors, we can analyze the helicity Raman intensity by Eq.(1.3). Firstly, we will define the helicity-conserved and helicity-changing Raman mode. For the helicity-conserved mode, it means that the incident light and the scattered light have the same helicity (both left-handed or right-handed). When the incident and scattered light are opposite to each other, this called the helicity-changing mode. In Fig.1.6, we show the schematic diagram for the helicity conserved and changing mode. In the Raman scattering, the incident light is left-handed polarized light (red line), when the scattered light is also left-handed (red line), this is the helicity-conserved mode. On the contrary, when scattered light is right-handed (blue line), this is helicity-changing mode.

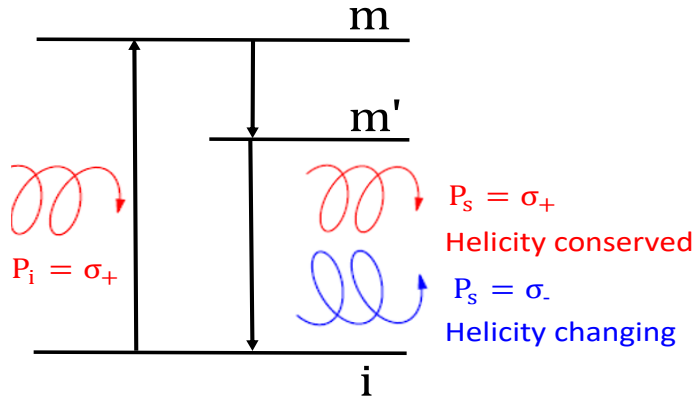


Figure 1.6 Schematic of helicity Raman spectra. The red line is the left-handed circularly polarized light (σ_+). The blue line is the right-handed circularly polarized light (σ_-).

The intensity for circular polarized Raman spectra is given by

$$I = |\sigma_{\pm}^* \cdot R(\nu) \cdot \sigma_{\pm}|^2. \quad (1.14)$$

Here, we show the expression of helicity Raman intensity by Eq.(1.14) for MoS_2 . Firstly, we can see intensity Table 1.1 for the E_{2g}^1 mode, when the incident light and scattered light are the same, Raman intensity is zero; On the contrary, Raman

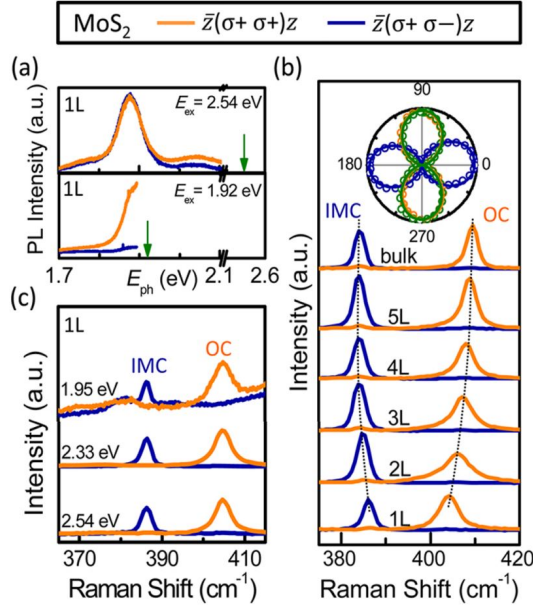
Intensity	σ_+	σ_-
σ_+	0	$ 2d' ^2, 2d ^2$
σ_-	$ 2d' ^2, 2d ^2$	0

Table 1.1: E_{2g}^1 mode helicity Raman intensity table

Intensity	σ_+	σ_-
σ_+	$ 2a ^2$	0
σ_-	0	$ 2a ^2$

Table 1.2: A_{1g} mode helicity Raman intensity table

intensity has specific value. We can conclude that the E_{2g}^1 mode is helicity-changing mode. As shown in Table 1.2 for the A_{1g} mode, when the incident light and scattered light are same, Raman intensity has specific value. This reveals that the A_{1g} mode is helicity-conserved mode. This property is controlled by the form of Raman tensor. In this thesis, we will achieve helicity Raman spectra numerically for LaAlSi in Chapter 3.

**Figure 1.7** Experimental results of helicity Raman spectra for MoS_2 . [26]

Chen et al. [26] observed the Raman spectra with circularly polarized light which

is shown in Fig.1.7. This is the Raman spectra of MoS₂ by using the helicity conserved (red lines) and changing (blue lines) configuration. For IMC (in-plane phonon), it is helicity-changing mode and OC (out-of-plane phonon) is helicity-conserved mode with changing laser energy and the number of layer. They showed the possibility to use circular polarized light to distinguish the phonon modes. However, the laser energy dependence of the Raman intensity in Fig.1.7(c) can not be explained by group theory. Therefore, the quantum expression of Raman tensor is needed, which will be introduced in Chapter 2.

1.3.4 Conservation law

The Rayleigh scattering is elastic scattering and the Raman scattering is inelastic scattering. In this section, the conservation law by using circular polarized light will be introduced, especially for the Raman scattering. By analyzing the conservation law, the phonon behavior in the circularly polarized Raman process will be explained, and we will introduce the prediction of the helicity-conserved and helicity-changing modes.

Firstly, we will briefly explain the Rayleigh scattering process. In the absorption process, an electron is excited by photon from valence band (i) to conduction band (m), $m_m - m_i = \sigma_i + Np_1$ ($p_1 = 0, \pm 1, \pm 2, \dots$); Then in the scattering process, the electron recombined with the hole in valence band and one photon is emitted, $m_f - m_m = -\sigma_s + Np_2$ ($p_2 = 0, \pm 1, \pm 2, \dots$). Here, m is the angular momentum, N is the symmetry of materials, σ_i (σ_s) is the spin angular momentum of incoming (scattering) photon. For the whole process of the Rayleigh scattering, $m_f - m_i = \sigma_i - \sigma_s + Np$ ($p = 0, \pm 1, \pm 2, \dots$). The initial state (i) and final state (f) are identical. Then it becomes $\sigma_s - \sigma_i = Np$ ($p = 0, \pm 1, \pm 2, \dots$). When the incident light and scattered light are same, $p=0$ satisfies the helicity conserved phenomenon for any symmetry. When the incident and scattered light are opposite, the four possibility are $N = 1, p = 2$ or -2 and $N = 2, p = 1$ or -1 . Therefore, only the one-fold and two-fold materials have the possibilities to achieve helicity changing behavior in Rayleigh scattering.

For Raman scattering, it is inelastic scattering. And there are three processes, which consists of:

Firstly, one electron is excited from initial state (i) to intermediate state (m), the conservation law is:

$$m_m - m_i = \sigma_i + Np_1 (p_1 = 0, \pm 1, \pm 2, \dots) \quad (1.15)$$

Secondly, a phonon is scattered, the conservation law is:

$$m'_m - m_m = -m_\nu^{ph} + N_\nu p_2 (p_2 = 0, \pm 1, \pm 2, \dots) \quad (1.16)$$

Thirdly, the electron recombined with hole on valence band (f) and emitted a photon, the conservation law is:

$$m_f - m'_m = -\sigma_s + Np_3 (p_3 = 0, \pm 1, \pm 2, \dots) \quad (1.17)$$

With combining the electron-phonon and electron-photon interactions, the conservation law is written by:

$$\sigma_s - \sigma_i = -m_\nu^{ph} + N_\nu p (p = 0, \pm 1, \pm 2, \dots) \quad (1.18)$$

For the helicity-conserved mode, when $p = 0$ and $m_\nu^{ph} = 0$, any N_ν is satisfied. MoS₂ is a three-fold material ($N = 3$), the symmetry of the E_{2g1} mode is one-fold ($N_\nu = 1$). When the incident light and scattered light are left-handed and right-handed polarized light respectively, $\sigma_i = 1, \sigma_s = -1$. In Eq.1.18, N_ν equals to 1, m_ν^{ph} equals to zero, and then when $p = -2$, the E_{2g1} mode is the helicity-changing mode. For six-fold material, graphene, E_{2g} mode is the helicity-changing mode with p equal to ± 1 . However, for two-fold and four-fold symmetry materials, there is no experimental results to support the helicity-changing behavior. In this thesis, we will give theoretical results for four-fold materials LaAlSi.

1.3.5 Weyl semimetal

Weyl semimetals (WSM) [27, 28] are one kind of materials that attracted much interests for its unique topological properties, which is similar with graphene upon breaking time-reversal or inversion symmetry. Although the Weyl fermions have been known for a long time, they were found in certain crystals in recent years [6]. In the WSM,

Symmetry	ν	N	N_ν	Degeneracy	m_ν^{ph}	p for the helicity change
D_{2h}	A_g	2	2	Nondegenerate	0	± 1
D_{2h}	B_{1g}	2	2	Nondegenerate	0	± 1
D_{3h}	E'	3	1	Degenerate	$0, \pm 1$	$\pm 1, \pm 2, \pm 3$
D_{4h}	B_{1g}	4	2	Nondegenerate	0	± 1
D_{4h}	B_{2g}	4	2	Nondegenerate	0	± 1
D_{6h}	E_{2g}	6	2	Degenerate	$0, \pm 1$	± 1

Figure 1.8 Conservation law for helicity changing Raman active mode [13]

it has the ‘Fermi arcs’, and it connected the Weyl points. As shown in Fig.1.9, we can see the Fermi arcs. [29] Raman spectra is a useful technique to recognize materials and study vibration and symmetry properties of different phonon modes. It provides a convenient and quick method to characterize samples simply. For the first-order Raman spectra, it is a single phonon process, only the Γ point ($q = 0$) phonon is emitted by considering momentum conservation law. The measured Raman spectra will be sensitive to phonon modes, laser energy and polarized light. For the WSM, the first-order Raman spectra can be used to characterize the lattice dynamics including symmetry of phonon modes. With this simple measurement, we can quickly know the phonon information. And study the laser energy dependent and polarization dependent properties. For WSM, in the case of LaAlSi/LaAlGe material, it shows important topological properties. However, the lattice dynamics, which has important role to study the structure, is still waiting for understanding. In this thesis, we will focus on the first-order resonant Raman spectra of LaAlSi.

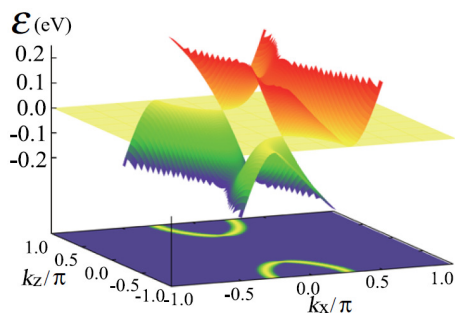


Figure 1.9 Weyl semimetal band structure diagram[29]

As shown in Fig.1.10, this is the crystal structure of LaAlSi. LaAlSi has tetragonal body center cubic structure, and characterized by point group C_{4v} and space group $I4_1md$. In the primitive cell, it contains 2 La atoms, 2 Al atoms and 2 Si atoms.

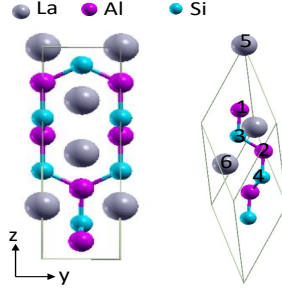


Figure 1.10 Crystal structure of LaAlSi calculated by Quantum ESPRESSO.

1.3.6 Experimental Results of resonant Raman spectra for LaAlSi

In this section, we show the experimental results of polarized Raman spectra for LaAlSi. As the candidate of WSM, its lattice dynamic properties are an important aspect to study. Therefore, Huang et al., studied the resonant Raman spectra of LaAlSi.

As shown in Fig.1.11, we show the polarized Raman intensity by using five laser energies for the A1 and B1 phonon modes. It reveals that the A1 mode at 195cm^{-1} and 422cm^{-1} is a circle, which means that Raman intensity is isotropic by changing polarized angle. And for the B1 mode at 120cm^{-1} , 295cm^{-1} and 378cm^{-1} show four-fold symmetry at 0 and 90 degree.

For the B1 mode at 296cm^{-1} , we can see the orange color plot in Fig.1.11, the phonon frequency has a shift by changing polarized angles. This is an irregular phenomenon which connects with the Weyl node of the WSM. And we will give possible explanations of frequency shift by Breit-Wigner-Fano lineshape and Kohn anomaly effect.

Fig. 1.9: Fig/weylBand.eps

Fig. 1.10: Fig/structure.pdf

Fig. 1.11: Fig/lasExperimental.pdf

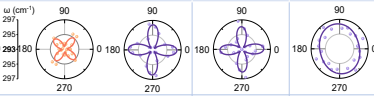
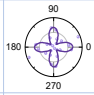
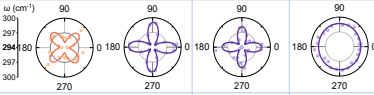
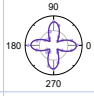
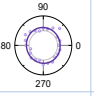
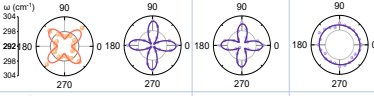
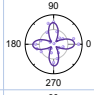
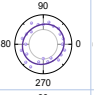
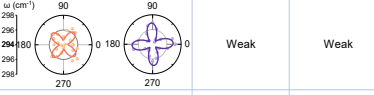
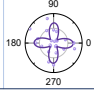
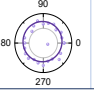
Raman mode	B_1^1	A_1^1	B_2^1	B_2^2	A_2^2
Experiment	120	195	295	378	422
Calculation	124.6	195.8	303.7	383.2	434.9
364 nm	Beyond detection limit	Weak			
488 nm		Weak			
532 nm					
633 nm				Weak	Weak
785 nm			Weak	Weak	Weak

Figure 1.11 Raman intensity and frequency shift with changing polarized angle.

Chapter 2

Methods of calculating resonant Raman intensity

In order to investigate the Raman spectra numerically, the electron-photon and electron-phonon interactions are important. Therefore, discussing the expression of electron-photon and electron-phonon interactions are essential for understanding the Raman process. In this chapter, we will give the derivation of Raman intensity formula. Meanwhile, discuss and explain the Raman tensor and Raman intensity of LaAlSi qualitatively.

2.1 Raman intensity

The first-order resonant Raman intensity is defined by[1, 30]:

$$I = \left| \sum_k \sum_{i=f,m,m'} \frac{M_{opt}^{fm'}(k) M_{ep,\nu}^{m',m}(k) M_{opt}^{mi}(k)}{(E_L - E^{mi}(k) - i\gamma)(E_L - E^{m'i}(k) - \hbar\omega_\nu - i\gamma)} \right|^2, \quad (2.1)$$

where M_{opt}^{mi} and $M_{opt}^{fm'}$ are electron-photon interaction matrix elements which represent the absorption process which is from the initial state (i) to the excited state (m), and scattering process from the intermediate state (m') to the final state (f), respectively. And $M_{ep,\nu}^{m',m}$ is the electron-phonon intereraction matrix element of the ν -th phonon mode. E_L is the incident laser energy; γ gives the resonance window. $E^{mi}(k)$ is the energy difference between the m and i state.

In order to calculate the Raman intensity of Eq.(2.1), matrix elements, M_{opt}^{mi} , $M_{opt}^{fm'}$ and $M_{ep,\nu}^{m',m}$, are the most important factors. In next section, we will discuss how to calculate matrix elements.

2.2 Electron-photon interaction by DFT

When the electrons are put in the electromagnetic field, the Hamiltonian is written by:

$$\begin{aligned} H &= \frac{1}{2m}(-i\hbar\nabla - e\mathbf{A})^2 + V(\mathbf{r}) + e\phi \\ &= \frac{1}{2m}(-\hbar^2\nabla^2 - ie\hbar\nabla \cdot \mathbf{A} - 2ie\hbar\mathbf{A} \cdot \nabla + e^2\mathbf{A}^2) + V(\mathbf{r}) + e\phi \end{aligned} \quad (2.2)$$

We consider Coulomb gauge ($\nabla \cdot \mathbf{A} = 0$) and make $\phi = 0$. And neglect the high order term (\mathbf{A}^2). Then Eq.2.2 is written by:

$$\begin{aligned} H &= \frac{1}{2m}(-\hbar^2\nabla^2 - ie\hbar\nabla \cdot \mathbf{A}) + V(\mathbf{r}) \\ &= -\frac{\hbar^2}{2m}\nabla^2 + V(\mathbf{r}) - \frac{ie\hbar}{m}\mathbf{A} \cdot \nabla \\ &= H_0 + H_{opt} \end{aligned} \quad (2.3)$$

For the perturbation term H_{opt} ,

$$H_{opt} = -\frac{ie\hbar}{m}\mathbf{A} \cdot \nabla \quad (2.4)$$

In the Maxwell equation,

$$\nabla \times \mathbf{B} = \mu_0 j + \mu_0 \varepsilon_0 \frac{\partial \mathbf{E}}{\partial t} \quad (2.5)$$

where $\mathbf{B} = \nabla \times \mathbf{A}$. And we consider charge density $j = 0$, then

$$\nabla \times \mathbf{B} = \nabla \times \nabla \times \mathbf{A} = \nabla(\nabla \cdot \mathbf{A}) - \Delta \mathbf{A} = \mu_0 \varepsilon_0 \frac{\partial \mathbf{E}}{\partial t} \quad (2.6)$$

The vector potential \mathbf{A} is defined by:

$$\mathbf{A} = \frac{i}{\omega} \sqrt{\frac{I_0}{c\varepsilon_0}} \exp(i(\mathbf{k}_{opt} \cdot \mathbf{r} \pm \omega t)) \mathbf{P} \quad (2.7)$$

Then the electron-photon matrix element M_{opt}^{fi} from initial state (i) to final state (f) is:

$$\begin{aligned}
M_{opt}^{fi} &= \langle f | H_{opt} | i \rangle \\
&= -\frac{ie\hbar}{m} \langle f | \mathbf{A} \cdot \nabla | i \rangle \\
&= \frac{e\hbar}{m\omega} \sqrt{\frac{I_0}{c\epsilon_0}} \exp(i(\omega_f - \omega_i \pm \omega)t) \langle f | \nabla | i \rangle \cdot \mathbf{P} \\
&= \frac{e\hbar}{m\omega} \sqrt{\frac{I_0}{c\epsilon_0}} \exp(i(\omega_f - \omega_i \pm \omega)t) \mathbf{D}^{fi} \cdot \mathbf{P}
\end{aligned} \tag{2.8}$$

where \mathbf{D}^{fi} is the dipole vector, and defined as below:

$$\mathbf{D}^{fi} = \langle f | \nabla | i \rangle \tag{2.9}$$

In Eq.(2.1), it gives the Raman intensity equation. For the electron-photon interaction $M_{opt} \propto \mathbf{D}^{fi} \cdot \mathbf{P}$, then Eq.(2.1) is written by:

$$\begin{aligned}
I &= \left| \sum_{\mathbf{k}} \sum_{i=f,m,m'} \frac{M_{opt}^{fm'}(\mathbf{k}) M_{ep,\nu}^{m',m}(\mathbf{k}) M_{opt}^{mi}(\mathbf{k})}{(E_L - E^{mi}(\mathbf{k}) - i\gamma)(E_L - E^{m'i}(\mathbf{k}) - \hbar\omega_\nu - i\gamma)} \right|^2 \\
&= |\mathbf{P}_s^* \cdot R \cdot \mathbf{P}_i|^2
\end{aligned} \tag{2.10}$$

where $R(\nu)$ is Raman tensor which is expressed by:

$$R(\nu) = \sum_{\mathbf{k}} \sum_{i=f,m,m'} \frac{\mathbf{D}_{opt}^{fm'}(\mathbf{k}) M_{ep,\nu}^{m',m}(\mathbf{k}) \mathbf{D}_{opt}^{mi}(\mathbf{k})^*}{(E_L - E^{mi}(\mathbf{k}) - i\gamma)(E_L - E^{m'i}(\mathbf{k}) - \hbar\omega_\nu - i\gamma)} \tag{2.11}$$

With dealing with electron-photon interaction, the Raman intensity can be expressed by Raman tensor $R(\nu)$. The wave function of initial and final states are calculated by first principle theory in Quantum ESPRESSO package. Then the dipole vector and electron-photon interaction matrix are calculated numerically.

2.3 Electron-phonon interaction by DFT

The atomic potential is changed by the vibration of neighbor atoms. Therefore the interactions between electron and ions are modified. We suppose the ion is located at

\mathbf{R}_s with a small displacement \mathbf{u}_s from equilibrium position \mathbf{R}_{s0} . Then the potential $V(\mathbf{r} - \mathbf{R}_s)$ is expressed by:

$$\begin{aligned} V(\mathbf{r} - \mathbf{R}_s) &= V(\mathbf{r} - \mathbf{R}_{s0} - \mathbf{u}_s) \\ &= V(\mathbf{r} - \mathbf{R}_{s0}) + \mathbf{u}_s \cdot \nabla_{\mathbf{u}_s} V(\mathbf{r} - \mathbf{R}_{s0} - \mathbf{u}_s)|_{\mathbf{u}_s=0} \\ &= V(\mathbf{r} - \mathbf{R}_{s0}) + \mathbf{u}_s \cdot \nabla_{\mathbf{R}_s} V(\mathbf{r} - \mathbf{R}_s)|_{\mathbf{R}_s=\mathbf{R}_{s0}} \end{aligned} \quad (2.12)$$

The electron-phonon matrix element with $q = 0$ phonon is expressed by:

$$M_{ep}^{fi}(\mathbf{k}, \mathbf{k}) = \sum_s \sqrt{\frac{\hbar}{2M_s\omega_\nu}} \langle \psi^f(\mathbf{k}, \mathbf{r}) | \mathbf{u}_s \cdot \nabla_{\mathbf{R}_s} V(\mathbf{r} - \mathbf{R}_s) |_{\mathbf{R}_s=\mathbf{R}_{s0}} | \psi^i(\mathbf{k}, \mathbf{r}) \rangle \quad (2.13)$$

where M_s is the mass of the ion at site s . We can calculate this electron-phonon matrix M_{ep}^{fi} by EPW package [31].

2.4 Raman tensor

As shown in Table 2.1, we give the character table of point group C_{4v} which LaAlSi belongs to. Only the phonon modes which has quadratic functions are Raman active modes. Therefore, in the table, A1 mode ($x^2 + y^2, z^2$), B1 mode ($x^2 - y^2$), B2 mode (xy) and E mode (xz, yz) are the Raman active modes. The Raman tensor can be written as:

$$R(E(xz, yz)) = \begin{pmatrix} 0 & 0 & xz \\ 0 & 0 & 0 \\ zx & 0 & 0 \end{pmatrix}, \begin{pmatrix} 0 & 0 & 0 \\ 0 & 0 & yz \\ 0 & zy & 0 \end{pmatrix}, \quad (2.14)$$

$$R(A1(x^2 + y^2, z^2)) = \begin{pmatrix} x^2 + y^2 & 0 & 0 \\ 0 & x^2 + y^2 & 0 \\ 0 & 0 & z^2 \end{pmatrix}. \quad (2.15)$$

$$R(B1(x^2 - y^2)) = \begin{pmatrix} x^2 - y^2 & 0 & 0 \\ 0 & -(x^2 - y^2) & 0 \\ 0 & 0 & 0 \end{pmatrix}. \quad (2.16)$$

We set $xz = zx = e(yz = zy = e)$, $x^2 + y^2 = a$, $z^2 = b$, $x^2 - y^2 = c$, then the Raman tensor has the format below:

$$R(E(xz, yz)) = \begin{pmatrix} 0 & 0 & e \\ 0 & 0 & 0 \\ e & 0 & 0 \end{pmatrix}, \begin{pmatrix} 0 & 0 & 0 \\ 0 & 0 & e \\ 0 & e & 0 \end{pmatrix}, \quad (2.17)$$

$$R(A1(x^2 + y^2, z^2)) = \begin{pmatrix} a & 0 & 0 \\ 0 & a & 0 \\ 0 & 0 & b \end{pmatrix}. \quad (2.18)$$

$$R(B1(x^2 - y^2)) = \begin{pmatrix} c & 0 & 0 \\ 0 & -c & 0 \\ 0 & 0 & 0 \end{pmatrix}. \quad (2.19)$$

Table 2.1: Character table of C_{4v} point group

C_{4v}	E	$2C_4(z)$	C_2	σ_v	σ_d	linear functions, rotations	quadratic functions	cubic functions
A_1	+1	+1	+1	+1	+1	z	$x^2 + y^2, z^2$	$z^3, z(x^2 + y^2)$
A_2	+1	+1	+1	-1	-1	R_z		
B_1	+1	-1	+1	+1	-1		$x^2 - y^2$	$z(x^2 - y^2)$
B_2	+1	-1	+1	-1	+1		xy	xyz
E	+2	0	-2	0	0	$(x, y)(R_x, R_y)$ (R_x, R_y)	(xz, yz)	(xz^2, yz^2) $(xy^2, x^2y)(x^3, y^3)$

After we know the Raman tensor of LaAlSi, we can analyze the Raman intensity for both linearly and circularly polarized light with Eq.(1.3).

With linearly polarized light, the geometry is set to parallel. When polarized vector is on the x direction, the polarized angle θ is zero degree.

We calculate the Raman intensity of LaAlSi qualitatively combining the polarized vector in Eq.(1.6) and Raman tensor. For the E mode, the Raman intensity equals to zero. For the A1 mode, the intensity equals to a^2 . And the Raman intensity of the B1 mode equals to $|c \cos(2\theta)|^2$. As shown in Fig.2.1, the left figure is the intensity of the A1 mode which gives a circle plot. This means the Raman intensity for the A1 mode is a constant with changing polarized angles. And the right figure shows the four-fold plot of the B1 mode.

Fig. 2.1: Fig/lasA1B1.eps

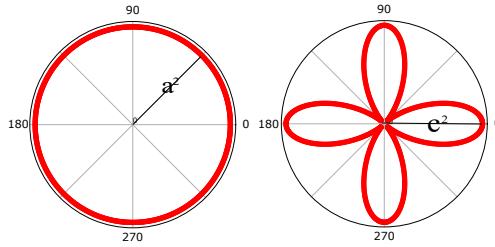


Figure 2.1 Polar plot of A1 and B1 mode for LaAlSi.

For the helicity Raman intensity, the polarized vectors are shown in Eq.(1.12) and Eq.(1.13). For the E mode, the Raman intensity equal to zero for both helicity-conserved and helicity-changing conditions. For the A1 and B1 modes, when the incident light and scattered light are both left-handed circularly polarized light, the Raman intensity is $|2a|^2$ and 0. And when helicity is opposite for incident and scattered light, the Raman intensity are 0 and $|2c|^2$ for the A1 and B1 modes, respectively. By analyzing the Raman intensity, the B1 is the helicity-changing mode, and A1 is helicity-conserved mode in LaAlSi.

Chapter 3

Resonant Raman spectra of LaAlSi

LaAlSi, as a candidate of the Weyl semimetal, shows some unusual behavior in the Raman spectra. In this section, firstly, we will discuss the polarized Raman spectra of LaAlSi and explain the irregular phenomenon of phonon frequency shift as function of polarized angle. Since LaAlSi is the Weyl semimetal, this also makes Kohn anomaly (KA) effect can happen around the Weyl nodes. Although KA effect can not explain the phonon frequency shift as a function of polarized angle, it can gives the clue of phonon frequency shift as a function of laser energy, which we will explain theoretically. Then, we discuss the circularly polarized Raman spectra of LaAlSi, which reveals the helicity-conserved and helicity-changing behavior of phonon modes.

3.1 Electronic properties of LaAlSi

LaAlSi, which is tetragonal body center cubic structure, is characterized by point group C_{4v} and space group $I4_1md$. As shown in Fig.(3.1), this is the energy dispersion of LaAlSi along high symmetry point Γ , X , Y , Σ , Γ , Z , Σ_1 and N , which are shown in the Brillouin zone. Fermi energy is put on 0 eV. By analyzing the band structure, LaAlSi has no band gap. Along Σ_1 and N point, there is a crossing point for valence band and conduction band, this is the so-called Weyl nodes.

In the primitive cell of LaAlSi, there are 6 atoms totally. In this case, there are 18 phonon modes. As shown in Fig.(3.2), this is the phonon dispersion which consists

Fig. 3.1: Fig/lasBands.pdf

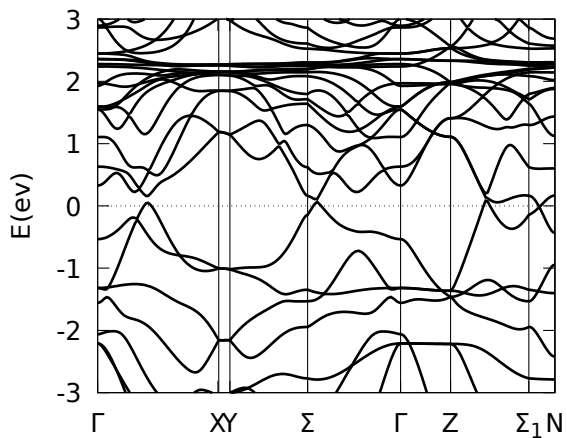


Figure 3.1 Band structure of LaAlSi along high symmetry point

of 3 acoustic phonon modes $[A_1+E]$ and 10 optical phonon modes $[2A_1+5E+3B_1]$, E modes are all degenerate. In Table 3.1, we show the phonon frequency at Γ point in the Brillouin zone. This corresponds to the Raman shift of phonon modes in the first-order Raman spectra.

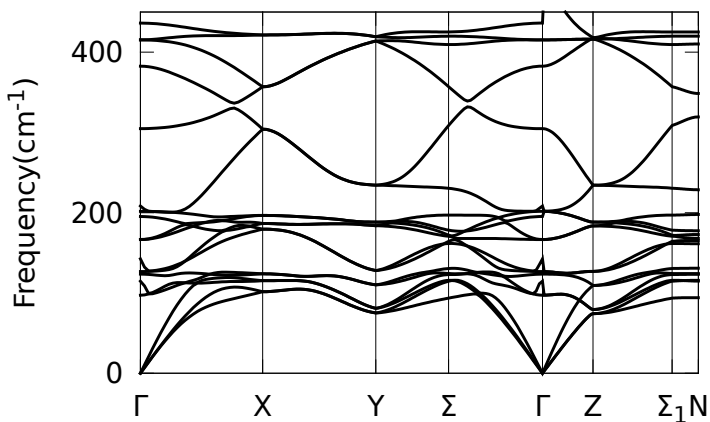


Figure 3.2 Optical phonon frequency of LaAlSi along high symmetry point

Phonon modes	E	B1	E	E	A1	E	B1	B1	E	A1
Frequency (cm ⁻¹)	109	124	132	170	196	202	303	383	411	434
Active	I+R	R	I+R	I+R	I+R	I+R	R	R	I+R	I+R

Table 3.1: Phonon frequency of LaAlSi at Γ point.

3.2 Polarized Raman spectra

In this section, we discuss the polarized Raman spectra of LaAlSi, and discuss the laser energy dependence of polarized Raman spectra. The geometry is parallel for all calculations below.

Firstly, we calculate the resonant Raman spectra of LaAlSi combined with DFT calculations. For LaAlSi, it has 15 optical phonon modes in first-order Raman spectra, which are the Raman active modes. Due to the Raman intensity of the E mode ($R(E(xz,yz))$) is zero in parallel configuration, it doesn't contribute to the Raman spectra. We will focus on the A1 and B1 modes in the discussion.

As shown in Fig.3.3, this is the calculated polarized Raman spectra by using five laser energies (785nm, 633nm, 533nm, 488nm and 364nm) at five polarization angles. In this figure, for the B1 mode at 303 cm⁻¹, the major peaks appear at 0 and 95 degree which show the same phenomenon for five laser energies. And the A1 mode at 434 cm⁻¹ shows same intensity with given five polarized angles. In order to know the angle and laser energy dependence of the symmetry for phonon modes, the polar plot of the Raman intensity is needed.

For the B1 mode at 124 and 383 cm⁻¹, the intensity is smaller compared with 303 cm⁻¹. And the A1 mode at 196cm⁻¹ is smaller compared with 434 cm⁻¹. We will not discuss here.

As shown in Fig.3.4, this is the polar plot of the Raman intensity as a function of polarized angles. By analyzing the Raman tensor of the A1 and B1 modes, we know that the Raman intensity is circle and four-fold symmetry, respectively. In our calculated results, we can see the polar plot for the B1 and A1 modes with five laser energies. For the B1 mode at 303 cm⁻¹, the main peaks of the Raman intensity appear at 0 and 90 degree by using laser energy 364, 488, 633 and 785nm, which is consistent

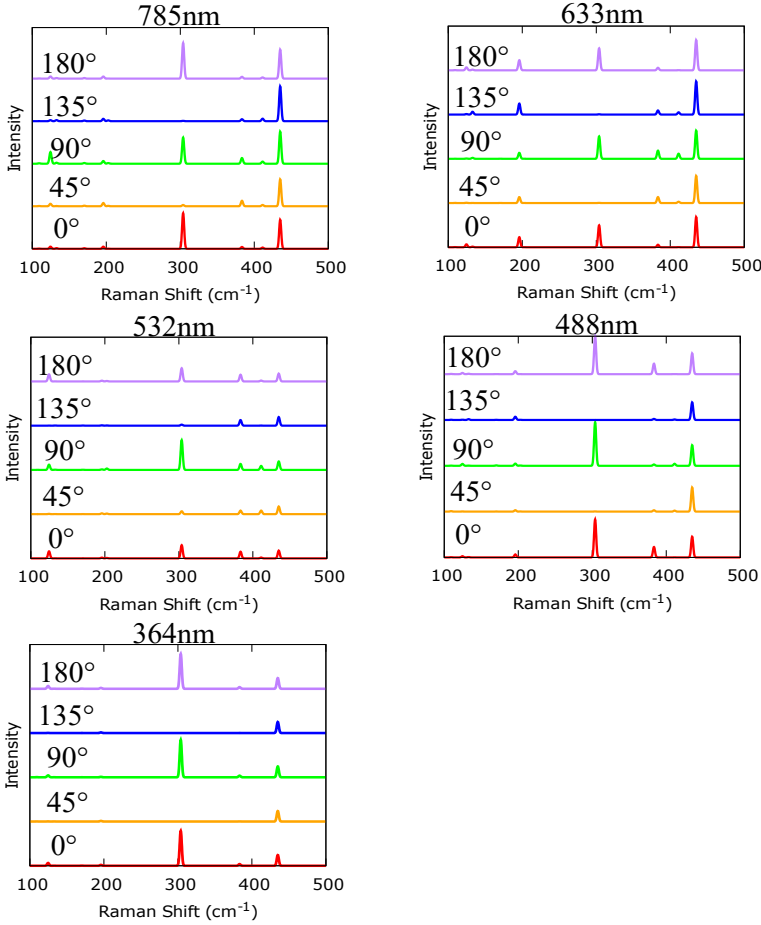


Figure 3.3 The calculated polarized Raman spectra of LaAlSi for five laser energies (364nm,488nm,532nm,633nm,785nm) at five angles (0, 45, 90, 135 and 180 degree).

with group theory analyse and experimental results. However, the polar plot of the Raman intensity loses four-fold symmetry at laser energy 532nm, which is coming from the interference effect between intermediate states. And the A1 mode at 434 cm⁻¹ by using laser energy 364nm has a circle plot with changing polarized angle. However, with changing laser energy, the polar plot transform to ellipse which has the same originate with the B1 mode.

In this section, we give the polarized Raman spectra and polar plot of Raman intensity. By analyzing, we can see the anisotropic properties of polarization dependence.

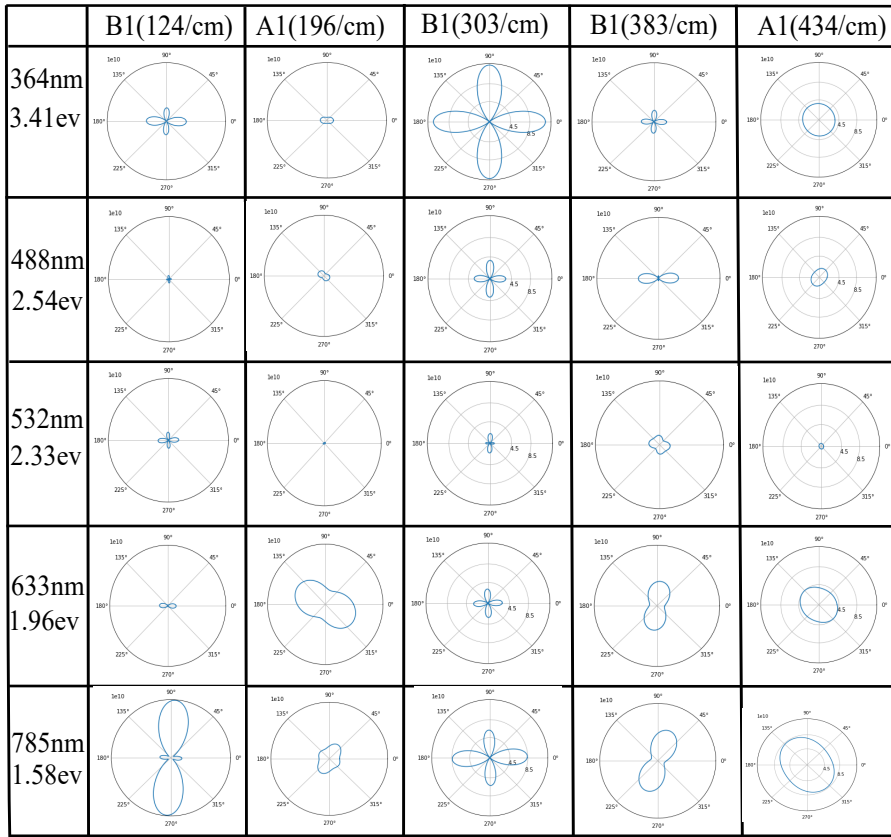


Figure 3.4 The calculated polar plot of Raman Intensity for LaAlSi with five laser energies (364nm,488nm,532nm,633nm,785nm) which contains five phonon modes (B1 mode at 124 cm^{-1} , A1 mode at 196 cm^{-1} , B1 mode at 303 cm^{-1} , B1 mode at 383 cm^{-1} , A1 mode at 434 cm^{-1})

This behavior depends on the Raman tensor format. For the resonant Raman spectra, our calculated results show laser energy dependence for the symmetry of phonon modes, which coming from γ value. However, the Raman spectra also give some irregular phenomenon that the Raman frequency gives a shift for the B1 phonon mode at 303 cm^{-1} . In next section, we will give the explanation of phonon frequency shift combined with Kohn anomaly effect and Breit-Wigner-Fano effect.

3.3 Phonon frequency shift

3.3.1 Kohn anomaly effect

In the Raman process, the emitted phonon will excite an electron-hole pair near the Weyl nodes. This phonon, which has energy $\hbar\omega_\nu$, will excite electrons near the Weyl nodes by electron-phonon interaction. Then the electron recombines with the hole and a phonon is emitted. As shown in Fig.3.5, this is so-called Kohn anomaly (KA) effect. When KA effect happens, the phonon frequency will be modified. However, by our analysis, KA effect can happen with the Weyl nodes accrossing the Fermi energy, it is not angle-dependent. Then we will explain the reason.

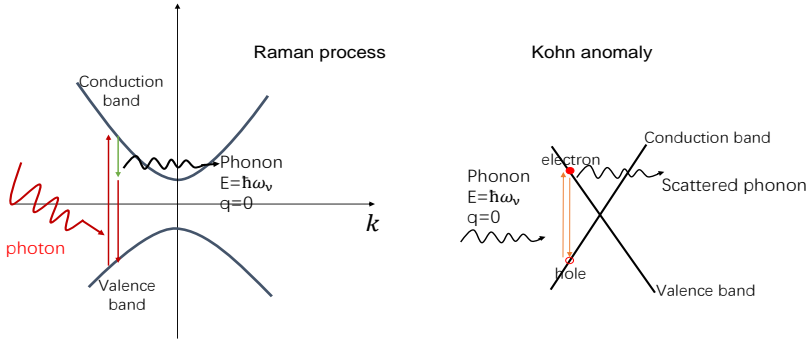


Figure 3.5 Raman spectra and Kohn anomaly effect.

The modification of frequency is written below:

$$\Delta\omega = \sum_k \frac{|M_{el-phonon}(k, k+q)|^2}{\hbar\omega_\nu - (E_c(k+q) - E_v(k)) + i\eta} \quad (3.1)$$

where $|M_{el-phonon}|^2$ is the electron-phonon interaction matrix element. ω_ν is the unperturbed phonon frequency. $\Delta\omega$ is the correction term of frequency.

With considering the KA effect, the phonon frequency will be modified. However, in the normal KA effect as we talked previously, the energy and wave vector for one specific phonon mode are constant with changing laser energy and polarized angle

when $q=0$. Therefore, the KA effect will become an invariant as a function of laser energy and polarized angle. Then we built a new model to explain that KA effect depends on the laser energy.

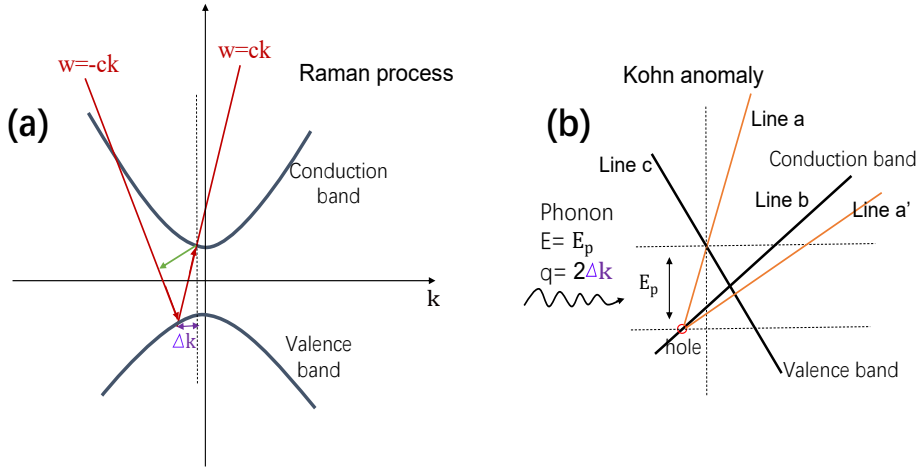


Figure 3.6 Raman spectra and Kohn anomaly effect with photon has momentum.

For the photon of the incident light in the Raman process, we neglect the momentum, and set the wave vector equal to zero. Nevertheless, we should consider the photon $\omega = ck$. Then the photon excited electron in the Raman process will not be excited vertically. As shown in Fig.3.6(a), the Raman process is modified. The scattered phonon have the momentum proportional to $2\Delta k$. And the coming phonon in KA effect will have the momentum. Then the electron in KA effect can not be excited vertically. Here, Δk is related to the laser energy. So, with this model, we can explain the laser energy dependence of the frequency shift.

Meanwhile, with the phonon having momentum, we can compare the group velocity to decide the KA effect can happen or not as shown in Fig.3.6(b), if the slope of a is larger than line b and c, then the electron can be excited and the KA effect can happen. As shown in Fig.3.7, this is the energy dispersion of LaAlSi acrossing Weyl node along k_z direction. We calculate the slope for line b and c, which is $3.7997 \times 10^5 m/s$ and $-10.014 \times 10^5 m/s$, respectively. On the other hand, at laser energy 2.33eV, the slope

Fig. 3.6: Fig/kohnQuan.eps

Fig. 3.7: Fig/slope.eps

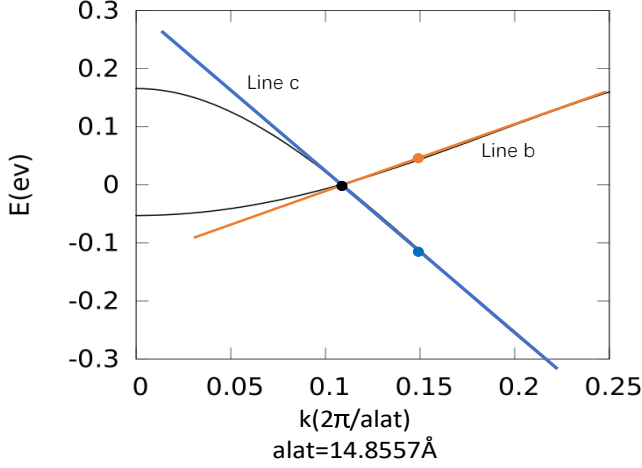


Figure 3.7 The energy dispersion of LaAlSi across Weyl node in the kz direction. The red and blue line are the linear approximation of band structure.

of excited electron for the B1 mode is $2.4185 \times 10^6 m/s$, which is larger than energy dispersion line b and c. Thus the KA effect can happen at laser energy 2.33eV.

However, for the normal KA effect, the electron-phonon interaction matrix element will be constant with changing polarized angle and laser energy. Even in the new model with considering the momentum, the momentum change $2\Delta k$ is related to the laser energy, but not the polarized angle. Therefore, with KA effect, the frequency shift as a function of polarized angle can not be explained. Only the laser energy dependence of frequency shift is given. In next section, we will use the Breit-Wigner-Fano effect to explain the possibilities of the Raman frequency shift.

3.3.2 Breit-Wigner-Fano effect

In Fano's paper, the interference of a discrete state with a continuum state leads to asymmetric spectra, this is known as the Breit-Wigner-Fano (BWF) lineshape [32]. In the Raman spectra, the discrete spectra coming from phonon excitation, and continuum spectra coming from electron excitation, this make BWF lineshape can happen in the Raman process.

The BWF lineshape is written as below:

$$I(\omega) = I_0 \frac{[1 + (\omega - \omega_{BWF})/q_{BWF}\Gamma]^2}{1 + [(\omega - \omega_{BWF})/\Gamma]^2} \quad (3.2)$$

where I_0 , ω , ω_{BWF} , q_{BWF} and Γ are the maximum intensity, the Raman shift, the peak position, the asymmetric factor, and the spectra width, respectively.

In Shengxi Huang's group, they observed the BWF feature of LaAlSi material, especially for the frequency shift phenomenon. In the experimental results, the frequency of the B1 mode is strongly depends on the polarized angle.

In order to get the relationship of the Raman frequency and asymmetric factor, we calculate the derivative of Eq.3.2 for the Raman shift ω . Then we get the relationship:

$$\frac{1}{q_{BWF}} = \frac{\omega - \omega_{BWF}}{\Gamma} \quad (3.3)$$

In this case, the Raman frequency depends on the q_{BWF} and Γ . If the q_{BWF} and Γ have polarized angles dependence, then the frequency shift can be explained. Now this work is in the progress.

3.4 Circularly polarized Raman spectra

In the Raman spectra, we always use the circularly polarized light as the light source. The geometry is $Z(\sigma_+\sigma_+)\bar{Z}$ and $Z(\sigma_+\sigma_-)\bar{Z}$. As shown in Fig.3.8, this is the circularly polarized Raman spectra of LaAlSi by using five laser energies. The green line means the incident light is left-handed circularly polarized light and scattered light is the right-handed circularly polarized light. The red line means the incident and scattered light are both left-handed circularly polarized light. By analyzing Fig.3.8, the B1 mode at 124 and 303 cm^{-1} has a green peak, which reveals the B1 mode is allowed only when incident and scattered light are opposite. Therefore, the B1 mode is helicity-changing mode. And for the A1 mode at 196 and 434 cm^{-1} , it gives a red peak, which show that the A1 mode is allowed only when incident and scattered light are both left or right-handed circularly polarized light, the A1 mode is the helicity-conserved mode. However, the B1 mode at 383 cm^{-1} shows helicity conserved behavior at laser energy 785, 633 and 532nm. At laser energy 488 and 364nm, it becomes helicity-changing mode, the reason is unclear now.

As we discussed in the Chapter 2, with considering the Raman tensor of LaAlSi, the B1 and A1 modes are the helicity changing and conserved mode, respectively. This is also consistent with prediction of conservation law.

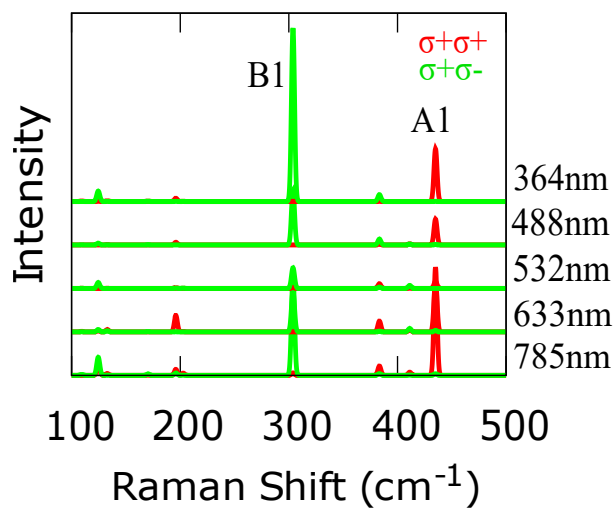


Figure 3.8 The calculated circularly polarized Raman spectra with laser energy 785, 633, 532, 488 and 364nm. The green line in the helicity-changing mode. The red line is the helicity-conserved mode.

Chapter 4

Conclusions

In this thesis, we discussed the polarized Raman spectra and helicity Raman spectra of the Weyl semimetal LaAlSi, especially the polarized Raman spectra.

For the polarized Raman spectra, we explained the polarization dependence of phonon symmetry. By combining with both group theory and experimental results, we analyze the calculated resonant Raman spectra, especially for the B1 and A1 modes. For the A1 mode, the intensity almost keep constant with changing polarized angles from 0 to 360 degree. And the polar plot gives the results of polarization dependence. For B1 mode, it gives a four-fold symmetry which the maximum intensity appear at 0 and 90 degree.

However, the material LaAlSi also show frequency shift behavior as a function of polarized angle for B1 mode in the Raman spectra. In this thesis, we use Kohn anomaly effect to explain the laser energy dependence of frequency shift. Meanwhile, the Breit-Wigner-Fano effect is one reason of the polarization dependence of the Raman frequency.

Meanwhile, in this thesis, we give the helicity Raman spectra of four-fold symmetry material LaAlSi. And both helicity-conserved and helicity-changing behavior are shown in this materials, which is consistent with the prediction of conservation law.

Appendix A

Input files for electron-photon and electron-phonon interaction matrix element

In this thesis, the numerical calculations are based on the Quantum ESPRESSO package, EPW (Electron-Phonon-Wannier) package, and our homemade program, the executable program is put in the home folder $\tilde{\text{~/opt/raman-tmp3/raman.x}}$. The input files are put in tube63, $\text{/abinitio/wangtong/espresso/las/}$. The electron-photon interaction, phonon calculation, epw calculation and Raman calculation are put in the folder ./elpt , ./phonon , ./epw and ./raman , respectively.

In order to calculate the Raman intensity, we have three steps.

Firstly, electron-photon interaction. Input files and commands are shown in Table.A.1.

Secondly, Γ point phonon. Input files and commands are shown in Table A.2.

Table A.1: Input files and commands for calculating electron-photon interaction.

step	Command	Input file	Output file
1.SCF calculation	pw.x	las.scf.in	las.scf.out
2.NSCF calculation	pw.x	las.nscf.in	las.nscf.out
		./wfc_save	./wfc_save
3.Output wavefunction	pw_export.x	pw_export.in	pw_export.out index.xml

Table A.2: Input files and commands for calculating Γ point phonon.

step	Command	Input file	Output file
1.SCF calculation	pw.x	las.scf.in	las.scf.out ./tmp
2.Phonon calculation	ph.x	las.ph.in ./tmp	las.ph.out ./tmp/_ph0/
3.Make input for EPW	python	pp.py ./tmp/_ph0/	./save

Thirdly, electron-phonon interaction. Input files and commands are shown in Table A.3.

Table A.3: Input files and commands for calculating electron-phonon interaction.

step	Command	Input file	Output file
1.SCF calculation	pw.x	las.scf.in	las.scf.out ./tmp
2.NSCF calculation	pw.x	las.nscf.in ./tmp	las.nscf.out ./tmp
3.Electron-phonon calculation	epw.x	epw.in ./tmp save	phband.dat ep_matele.dat

Fourthly, Raman intensity. Input files and commands are shown in Table A.4.

Table A.4: Input files and commands for calculating Raman intensity.

step	Command	Input file	Output file
Raman calculation	Raman.x	raman.in index.xml phband.dat ep_matele.dat	raman.out

Then, we will give the details of input files.

A.0.1 Input files based on Quantum espresso

```
las.scf.in:
```

```
*****
```

```
&control
```

```
  calculation = 'scf'
```

```
  verbosity = 'high'
```

```
restart_mode = 'from_scratch'
wf_collect = .true.
  nstep = 200
  tstress = .true.
  tprnfor = .true.
etot_conv_thr = 1.0E-6
forc_conv_thr = 1.0D-5
pseudo_dir = './../pp'
  outdir = './wfc_save/'
  prefix = 'las'
/
&system
  ibrav = 0
  nat = 6
  ntyp = 3
  nbnd = 80
  ecutwfc = 180
  occupations='smearing'
  smearing='m-p'
  degauss=0.01
/
&electrons
  conv_thr = 1.0d-8
  mixing_beta = 0.10
/
&ions
  ion_dynamics = 'bfgs'
/
&cell
  cell_dynamics = 'bfgs'
  press_conv_thr = 0.01
/
ATOMIC_SPECIES
Al 26.98154 13_Al.upf
Si 28.08550 14_Si.upf
```

La 138.9055 57_La.upf

ATOMIC_POSITIONS (crystal)

Al	0.582784214	0.582784214	0.000000000	! // Al
Al	0.332784214	0.832784214	0.500000000	! // Al
Si	0.416358551	0.416358551	-0.000000000	! // Si
Si	0.166358551	0.666358551	0.500000000	! // Si
La	0.999157235	0.999157235	0.000000000	! // La
La	0.749157235	0.249157235	0.500000000	! // La

CELL_PARAMETERS (angstrom)

-2.121731571	2.121731571	7.266101132
2.121731571	-2.121731571	7.266101132
2.121731571	2.121731571	-7.266101132

K_POINTS (automatic)

6 6 0 0 0

las.nscf.in:

&control

```

    calculation = 'nscf'
    verbosity = 'high'
    restart_mode = 'from_scratch'
    wf_collect = .true.
    nstep = 200
    tstress = .true.
    tprnfor = .true.
    etot_conv_thr = 1.0E-6
    forc_conv_thr = 1.0D-5
    pseudo_dir = './.././pp'
    outdir = './wfc_save/'
    prefix = 'las'

```

/

&system

ibrav = 0

```

        nat = 6
        ntyp = 3
        nbnd = 80
        ecutwfc = 180
        occupations='smearing'
        smearing='m-p'
        degauss=0.01
        nosym=.true.
        noinv=.true.
/
&electrons
        conv_thr = 1.0d-8
        mixing_beta = 0.10
/
&ions
        ion_dynamics = 'bfgs'
/
&cell
        cell_dynamics = 'bfgs'
        press_conv_thr = 0.01
/
ATOMIC_SPECIES
Al 26.98154 13_Al.upf
Si 28.08550 14_Si.upf
La 138.9055 57_La.upf
ATOMIC_POSITIONS (crystal)
Al      0.582784214    0.582784214    0.000000000    ! // Al
Al      0.332784214    0.832784214    0.500000000    ! // Al
Si      0.416358551    0.416358551   -0.000000000    ! // Si
Si      0.166358551    0.666358551    0.500000000    ! // Si
La      0.999157235    0.999157235    0.000000000    ! // La
La      0.749157235    0.249157235    0.500000000    ! // La
CELL_PARAMETERS (angstrom)
-2.121731571    2.121731571    7.266101132
 2.121731571   -2.121731571    7.266101132

```

```

    2.121731571    2.121731571   -7.266101132
K_POINTS (automatic)
12 12 12 0 0 0

```

```
*****
```

```
pw_export.in :
```

```
*****
```

```
&INPUTPP
```

```

    prefix = 'las'
    outdir = './wfc_save/'
    pseudo_dir = '../..pp/'
    ascii = .TRUE.
    single_file = .TRUE.

```

```
/
```

```
*****
```

```
las.ph.in ::
```

```
*****
```

```
&inputph
```

```

    prefix = 'las',
    epsil = .true.,
    amass(1) = 26.98154,
    amass(2) = 28.08550,
    amass(3) = 138.9055,
    tr2_ph = 1.0d-18,
    outdir = './tmp/',
    fildyn = 'las.dyn',
    fildvscf = 'dvscf',
    ldisp = .true.,
    trans = .true.
    nq1 = 1,
    nq2 = 1,
    nq3 = 1,

```

```
/
```

```
*****
```

```
las.epw.in:
```

```
*****
```

```
&inputepw
```

```
prefix      = 'las '  
amass(1)    = 26.98154  
amass(2)    = 28.08550  
amass(3)    = 138.9055  
outdir      = './tmp/'
```

```
elph        = .true.  
kmaps       = .false.  
etf_mem     = 2
```

```
epbwrite    = .true.  
epbread     = .false.
```

```
epwwrite    = .true.  
epwread     = .false.
```

```
nbndsub     = 32  
nbndskip    = 0
```

```
wannierize  = .true.  
num_iter    = 5000  
iprint      =2  
dis_win_max =20.0  
dis_win_min = 0.0  
dis_froz_max =13.5  
dis_froz_min =7.5
```

```
proj(1)     = 'Al:s '  
proj(2)     = 'Al:px'
```

```

proj(3)      = 'Al:py'
proj(4)      = 'Al:pz'
proj(5)      = 'Si:s'
proj(6)      = 'Si:px'
proj(7)      = 'Si:py'
proj(8)      = 'Si:pz'
proj(9)      = 'La:px'
proj(10)     = 'La:py'
proj(11)     = 'La:pz'
proj(12)     = 'La:dz2'
proj(13)     = 'La:dx2-y2'
proj(14)     = 'La:dxy'
proj(15)     = 'La:dyz'
proj(16)     = 'La:dxz'

wdata(1)     = 'bands_plot = .true.'
wdata(2)= 'begin kpoint_path'
wdata(3)= 'G  0.000000  0.000000  0.000000
           X -0.500000  0.500000  0.000000'
wdata(4)= 'X -0.500000  0.500000  0.000000
           Y -0.500000  0.500000 -0.046230'
wdata(5)= 'Y -0.500000  0.500000 -0.046230
           S -0.271320  0.271320 -0.271320'
wdata(6)= 'S -0.271320  0.271320 -0.271320
           G  0.000000  0.000000  0.000000'
wdata(7)= 'G  0.000000  0.000000  0.000000
           Z  0.500000  0.500000 -0.500000'
wdata(8)= 'Z  0.500000  0.500000 -0.500000
           S1 0.271320  0.728680 -0.728680'
wdata(9)= 'S1 0.271320  0.728680 -0.728680
           N -0.000000  0.500000 -0.500000'
wdata(10)= 'N -0.000000  0.500000 -0.500000
            P -0.250000  0.750000 -0.250000'
wdata(11)= 'P -0.250000  0.750000 -0.250000
            Y1 0.042630  0.957370 -0.500000'

```



```

wdata(12)= 'Y1 0.042630 0.957370 -0.500000
           Z 0.500000 0.500000 -0.500000'
wdata(13)= 'X -0.500000 0.500000 0.000000
           P -0.250000 0.750000 -0.250000'
wdata(14)= 'end kpoint_path'
wdata(15)= 'bands_plot_format = gnuplot'
wdata(16)= 'guiding_centres=true'
wdata(17)= 'conv_tol= 1d-12'
wdata(18)= 'conv_window=20'
wdata(19)= 'dis_conv_tol=1d-12'
wdata(20)= 'dis_conv_window=9'

iverbosity = 3

elecselken = .true.
phonselken = .false.
a2f         = .false.

fsthick     = 6.0 ! eV
eptemp      = 300 ! K (same as PRB 76, 165108)
degaussw    = 0.01 ! eV

efermi_read =.true.
fermi_energy =10.840
band_plot   =.true.

dvscf_dir   = '../phonon/save/'
filkf       = 'meshes/pathk16.dat'
filqf       = 'meshes/pathq.dat'

nk1         = 10
nk2         = 10
nk3         = 10

nq1         = 1

```

```

nq2          = 1
nq3          = 1

/
  1 cartesian
  0.0000000000000000E+00  0.0000000000000000E+00  0.0000000000000000E+00
1.0
*****

raman.in :
*****
&inputraman
  prefix = 'las'
  outdir = './raman'
  sorb = .FALSE.
  circular_pol = .TRUE.
  nonpol = .TRUE.
  input_pw_export = './index.xml'
  fil_phband = './phband.freq'
  fil_matele_elph = './ep_matele.dat'
  gamma = 0.1d0
  gamma_raman = 0.0002d0
  nbv = 10
  nscf_occ = 26
  nqs = 1
  nmode = 18
  elaser1 = 1.58d0
  elaser2 = 1.96d0
  elaser3 = 2.33d0
  elaser4 = 2.54d0
  elaser5 = 3.41d0
  nrs = 5000
  n_kinterp = 3
  rs_start = 0.00d0

```

```
        rs_end = 0.01d0
!   plot_matele_elph = .TRUE.
!   plot_matele_opt = .TRUE.
!       plot_raman_k = .TRUE.
/
*****
```


Publication list

Papers

1. Kunyan Zhang, Xiaoqi Pang, **Tong Wang**, Fei Han, Shun-Li Shang, Nguyen T. Hung, Ahmad R. T. Nugraha, Zi-Kui Liu, Mingda Li, Riichiro Saito, and Shengxi Huang, Anomalous phonon-mode dependence in polarized Raman spectroscopy of the topological Weyl semimetal TaP, Phys. Rev. B 101, 014308, 2020.

Conferences

Oral presentations

1. **T. Wang**, Nguyen T. Hung, A. R. T. Nugraga and R. Saito. Why does helicity of a phonon mode change in Raman spectroscopy of MoS₂. Presented in ATI Zao-meeting, (August 05-06, 2019), Zao-Yamagata, Japan.

Poster Presentations

1. **T. Wang**, Nguyen T. Hung, A. R. T. Nugraga and R. Saito. Angle-Dependent Resonant Raman spectra of LaAlSi. The 56th Fullerenes, Nanotubes and Graphene General Symposium (March 02-04, 2019), Nagoya University, Tokyo, Japan.
2. **T. Wang**, Nguyen T. Hung, A. R. T. Nugraga and R. Saito. Laser-energy dependence helicity-changing Raman spectra of MoS₂. The 57th Fullerenes, Nanotubes and Graphene General Symposium (September 03-05, 2019), Nagoya University, Nagoya, Japan.

3. **T. Wang**, X. Q. Pang, Nguyen T. Hung, A. R. T. Nugraga, K. Zhang, S. Huang and R. Saito. First-order resonant Raman spectra of Weyl semimetal LaAlSi. The 3rd Symposium for the Core Research Clusters for Materials Science and Spintronics (February 10-11, 2020), Sendai International Center, Sendai, Japan.

Bibliography

- [1] MS Dresselhaus, G. Dresselhaus, R. Saito, and A. Jorio, *Physics Reports* 409(2), 47 – 99 (2005).
- [2] Andrea C Ferrari, JC Meyer, Vittorio Scardaci, Cinzia Casiraghi, Michele Lazzeri, Francesco Mauri, Stefano Piscanec, Da Jiang, KS Novoselov, S Roth, et al., *Physical review letters* 97(18), 187401 (2006).
- [3] A Jorio, R Saito, JH Hafner, CM Lieber, DM Hunter, T McClure, G Dresselhaus, and MS Dresselhaus, *Physical Review Letters* 86(6), 1118 (2001).
- [4] R Trommer and M Cardona, *Physical Review B* 17(4), 1865 (1978).
- [5] X. Wan, A. M. Turner, A. Vishwanath, and S. Y. Savrasov, *Physical Review B* 83(20), 205101 (2011).
- [6] S. Xu, I. Belopolski, N. Alidoust, M. Neupane, G. Bian, C. Zhang, R. Sankar, G. Chang, Z. Yuan, C. Lee, et al., *Science* 349(6248), 613–617 (2015).
- [7] B. Q. Lv, H. M. Weng, B. B. Fu, X. P. Wang, H. Miao, J. Ma, P. Richard, X. C. Huang, L. X. Zhao, G. F. Chen, Z. Fang, X. Dai, T. Qian, and H. Ding, *Physical Review X* 5(3), 031013 (2015).
- [8] R. G. Parr. Density functional theory of atoms and molecules. In *Horizons of Quantum Chemistry*, pages 5–15, Springer, 1980.
- [9] K. Burke, *The Journal of chemical physics* 136(15), 150901 (2012).
- [10] T. N. Yu, J. Yuan, Y. Luo, Y. Wu, and L. Shen, arXiv preprint arXiv:2005.05560 (2020).

- [11] Daniel S Sanchez, Su-Yang Xu, Nasser Alidoust, Guoqing Chang, Hong Lu, Bahadur Singh, Ilya Belopolski, Xiao Zhang, Guang Bian, Hao Zheng, et al., APS 2017, L44–002 (2017).
- [12] Arnold M Guloy and John D Corbett, *Inorganic Chemistry* 30(25), 4789–4794 (1991).
- [13] Y. Tatsumi, T. Kaneko, and R. Saito, *Phys. Rev. B* 97, 195444 (May 2018).
- [14] Zhonghua Yu and Louis Brus, *The Journal of Physical Chemistry B* 105(6), 1123–1134 (2001).
- [15] A. G. Souza Filho, S. G. Chou, G. G. Samsonidze, G Dresselhaus, MS Dresselhaus, L. An, J. Liu, A. K. Swan, MS Unlu, BB Goldberg, A. Jorio, A. Gruneis, and R. Saito, *Physical Review B* 69(11), 115428 (2004).
- [16] K. Kneipp, H. Kneipp, P. Corio, S. D. M. Brown, K. Shafer, J. Motz, L. T. Perelman, E. B. Hanlon, A. Marucci, G. Dresselhaus, and M. S. Dresselhaus, *Physical review letters* 84(15), 3470 (2000).
- [17] G. S. Duesberg, I. Loa, M. Burghard, K. Syassen, and S. Roth, *Physical review letters* 85(25), 5436 (2000).
- [18] LG Cançado, MA Pimenta, BRA Neves, G Medeiros-Ribeiro, Toshiaki Enoki, Yousuke Kobayashi, Kazuyuki Takai, Ken-ichi Fukui, MS Dresselhaus, R Saito, et al., *Physical review letters* 93(4), 047403 (2004).
- [19] S. Kim, K. Kim, J-U. Lee, and H. Cheong, *2D Materials* 4(4), 045002 (2017).
- [20] Y. Tatsumi and R. Saito, *Physical Review B* 97(11), 115407 (2018).
- [21] Yanlong Wang, Chunxiao Cong, Caiyu Qiu, and Ting Yu, *small* 9(17), 2857–2861 (2013).
- [22] X Zhang, WP Han, JB Wu, Silvia Milana, Y Lu, QQ Li, AC Ferrari, and PH Tan, *Physical Review B* 87(11), 115413 (2013).
- [23] J. Ribeiro-Soares, R. M. Almeida, E. B. Barros, P. T. Araujo, M. S. Dresselhaus, L. G. Cancado, and A. Jorio, *Physical Review B* 90(11), 115438 (2014).

- [24] W. Zhao, Z. Ghorannevis, K. K. Amara, J. R. Pang, M. Toh, X. Zhang, C. Kloc, P. H. Tan, and G. Eda, *Nanoscale* 5(20), 9677–9683 (2013).
- [25] Y. Yang, R. C. Da Costa, M. J Fuchter, and A. J. Campbell, *Nature Photonics* 7(8), 634–638 (2013).
- [26] S. Chen, C. Zheng, M. S. Fuhrer, and J. Yan, *Nano letters* 15(4), 2526–2532 (2015).
- [27] Shin-Ming Huang, Su-Yang Xu, Ilya Belopolski, Chi-Cheng Lee, Guoqing Chang, BaoKai Wang, Nasser Alidoust, Guang Bian, Madhab Neupane, Chenglong Zhang, et al., *Nature communications* 6(1), 1–6 (2015).
- [28] LX Yang, ZK Liu, Yan Sun, Han Peng, HF Yang, Teng Zhang, Bo Zhou, Yi Zhang, YF Guo, Marein Rahn, et al., *Nature physics* 11(9), 728–732 (2015).
- [29] M. Udagawa and E. J. Bergholtz, *Phys. Rev. Lett.* 117, 086401 (Aug 2016).
- [30] R. Saito, M. Hofmann, G. Dresselhaus, A. Jorio, and MS. Dresselhaus, *Advances in Physics* 60(3), 413–550 (2011).
- [31] J. Noffsinger, F. Giustino, B. D. Malone, C. H. Park, S. G. Louie, and M. L. Cohen, *Computer Physics Communications* 181(12), 2140–2148 (2010).
- [32] Ugo Fano, *Physical Review* 124(6), 1866 (1961).